Interactions of Conformationally Biased North and South 2′-Fluoro-2′,3′-dideoxynucleoside 5′-Triphosphates with the Active Site of HIV-1 Reverse Transcriptase

Lan Mu,[‡] Stefan G. Sarafianos,[||] Marc C. Nicklaus,[‡] Pamela Russ,[‡] Maqbool A. Siddiqui,[‡] Harry Ford Jr.,[‡] Hiroaki Mitsuya,[§] Richard Le,[§] Eiichi Kodama,[§] Chris Meier,[⊥] Tina Knispel,[⊥] Lynne Anderson,[‡] Joseph J. Barchi Jr.,[‡] and Victor E. Marquez*[,‡]

Laboratory of Medicinal Chemistry, Division of Basic Sciences, and Experimental Retrovirology Section, Medicine Branch, Division of Clinical Sciences, National Cancer Institute, National Institutes of Health, Bethesda, Maryland 20892, and Center for Advanced Biotechnology and Medicine and Rutgers University Chemistry Department, 679 Hoes Lane Piscataway, New Jersey 08854, and Institute of Organic Chemistry, University of Hamburg, Martin-Luther-King-Platz 6, D-20146 Hamburg, Germany

Received May 12, 2000; Revised Manuscript Received June 26, 2000

ABSTRACT: Molecular dynamics simulations of a ternary complex of HIV-1 reverse transcriptase (RT), double-stranded DNA, and bound dideoxynucleoside-5′-triphosphate (RT−DNA−ddNTP), utilizing the ddNTPs ddATP, βFddATP, and αFddATP, explain the experimentally observed order of potency of these 5′-triphosphates as inhibitors of RT: ddATP > βFddATP > αFddATP. On the basis of RT's known preference to bind the incoming dNTP (or ddNTP) with a north conformation at the polymerase site, αFddATP, which in solution prefers almost exclusively a north conformation, was predicted to be the most potent inhibitor. However, Tyr115, which appears to function as a steric gate to preclude the binding of ribonucleoside 5′-triphosphates, prevents the effective binding of αFddATP in its preferred north conformation. The south-biased βFddATP, while able to bind to RT without hindrance by Tyr115, has to pay a high energy penalty to be flipped to the active north conformation at the polymerase site. Finally, the more flexible and less conformationally biased ddATP is able to switch to a north conformation at the RT site with a smaller energy penalty than βFddATP. These results highlight the opposite conformational preferences of HIV-1 RT for αFddATP and βFddATP and help establish conformational guidelines for optimal binding at the polymerase site of this enzyme.

Our laboratory in collaboration with other investigators has begun a systematic study of the role of the sugar ring in the process of recognition and binding of nucleosides, nucleotides, and oligonucleotides by various enzymes (*1*−*15*). The emerging picture from these studies is that the majority of enzymes appear to have strict conformational requirements for substrate binding with the furanose ring in a well-defined shape. For nucleosides, four conformational parameters are critical for describing shape. These are (i) the glycosyl torsion angle χ (Figure 1, panels A and B), which determines the syn or anti disposition of the base relative to the sugar moiety; (ii) the torsion angle γ (Figure 1, panels A−C), which determines the orientation of the 5′-OH with respect to C3′ as represented by the three main rotamers: +*sc*, *ap*, −*sc*; (iii) the puckering of the furanose ring described by the phase angle of pseudorotation P (0−360°, Figure 1D); and (iv) the deviation from planarity of the furanose ring indicated by the maximum out-of-plane pucker ν_{max} ($\nu_{max} = \nu_2/\cos P$) (*16*, *17*). The value of P depends on the five endocyclic sugar torsion angles $\nu_0-\nu_4$ (Figure 1D) according to the following relationship: $\tan P = (\nu_4 + \nu_1) - (\nu_3 + \nu_0)/2\nu_2$ ($\sin 36° + \sin 72°$). By convention, a phase angle $P = 0°$ is set to correspond to an absolute north conformation possessing a symmetrical twist form $^3T_2$. Its south antipode, $_3T^2$, is represented by $P = 180°$. In practically all nucleosides, the value of P normally falls in a tight range close to either a $^3T_2$ (north) conformation or a $_3T^2$ (south) conformation (*17*). While in the solid state only one of these forms predominates, in solution the two conformations appear to exist in a rapid dynamic equilibrium dictated by the balance of stereoelectronic gauche and anomeric effects, which are in turn influenced by the electronegativity, ionization state, steric bulk, and relative configuration of all the substituents on the sugar ring (*18*).

The role of fluorine substitution on the sugar moiety has been the focus of attention of many studies attempting to correlate the fluorine-induced sugar pucker with associated biological activities in various nucleoside systems (*19*). By virtue of being the most electronegative of substituents, a fluorine atom can exert a powerful influence on the preferred mode of sugar pucker as confirmed by X-ray crystallography in the solid state (*20*−*27*) and by NMR measurements in solution (*13*, *19*, *28*, *29*). One of the most striking examples in support of the important role of fluorine was demonstrated

* To whom correspondence should be addressed.
[‡] Laboratory of Medicinal Chemistry, National Institutes of Health.
[§] Experimental Retrovirology Section, National Institutes of Health.
[||] Center for Advanced Biotechnology and Medicine and Rutgers University Chemistry Department.
[⊥] University of Hamburg.

10.1021/bi001090n
Published on Web 08/19/2000

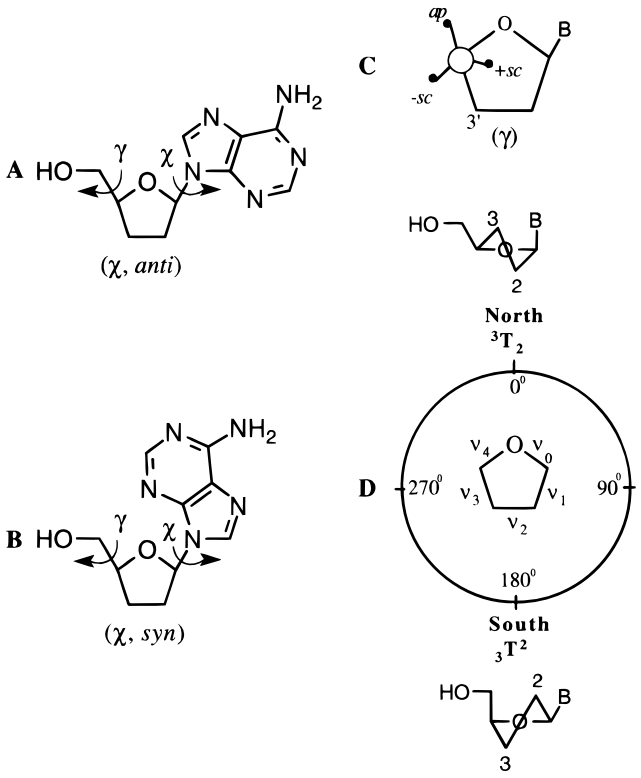

FIGURE 1: (Panels A and B) Definition of anti and syn conformations for a purine nucleoside; χ is defined as torsion angle O4′−C1′−N9−C4. (C) Definition of the torsion angle ranges for γ about the C4′−C5′ bond. (D) Pseudorotational cycle of the furanose ring in nucleosides.

in our early studies designed to overcome the acid lability of the glycosyl bond of two anti-HIV active purine dideoxynucleosides: dideoxyadenosine (ddA) and dideoxyinosine (ddI, Videx) (*30*, *31*). A major problem with these drugs is that their extreme acid instability makes them unsuitable for oral administration without prior neutralization of stomach acids. Since acid-catalyzed hydrolysis of purine nucleosides proceeds through a mechanism in which the protonated nucleoside dissociates into a glycosyl carbocation and free purine, the incorporation of fluorine at position C2′—adjacent to the reaction center—destabilizes the resulting oxocarbenium ion-like transition state and significantly decreases the rate of hydrolysis (*30*, *31*). Indeed, both 2′-fluoro diastereoisomers, 9-(2′,3′-dideoxy-2′-fluoro-β-D-*erythro*-pentofuranosyl)adenine (αFddA, **1**)[1] and 9-(2′,3′-dideoxy-2′-fluoro-β-D-*threo*-pentofuranosyl)adenine (βFddA, **2**) are extremely stable at pH 1 (*30*, *31*). Surprisingly, however, despite their

[1] Abbreviations: ADA, adenosine deaminase; AZT, 3′-deoxy-3′-azidothymidine; AZTTP, 3′-deoxy-3′-azidothymidine-5′-triphosphate; αFddA, 9-(2′,3′-dideoxy-2′-fluoro-β-D-*erythro*-pentofuranosyl)adenine; βFddA, 9-(2′,3′-dideoxy-2′-fluoro-β-D-*threo*-pentofuranosyl)adenine; αFddATP, 9-(2′,3′-dideoxy-2′-fluoro-β-D-*erythro*-pentofuranosyl)adenine-5′-triphosphate; βFddATP, 9-(2′,3′-dideoxy-2′-fluoro-β-D-*threo*-pentofuranosyl)adenine-5′-triphosphate; CHARMm, Chemistry at Harvard Molecular mechanics; ddA, 2′,3′-dideoxyadenosine; ddI, 2′,3′-dideoxyinosine; ddATP, 2′,3′-dideoxyadenosine-5′-triphosphate; ddNTP, 2′,3′-dideoxynucleoside-5′-triphosphate; dNTP, 2′-deoxynucleoside-5′-triphosphate; dCK, deoxycytidine kinase; DMP, decay per minute; EGTA, ethylene glycol-bis{amino ethyl ether} *N*,*N*, *N*′*N*′-tetra acetic acid; HIV, human immunodeficiency virus; HPLC, high-pressure liquid chromatography; NMR, nuclear magnetic resonance; PDB, Protein Data Base; RT, reverse transcriptase; TEAB, triethylammonium bicarbonate; TMP, thymidine-5′-monophosphate; UV, ultraviolet; VT, variable temperature.

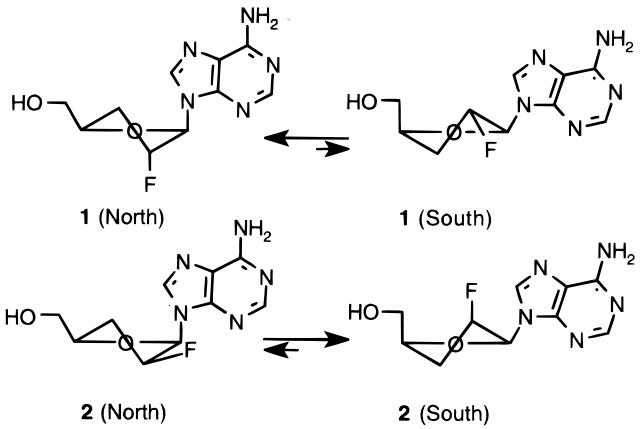

FIGURE 2: Structures of αFddA (**1**) and βFddA (**2**) showing their conformational preferences in solution.

structural similarity to ddA, only βFddA displayed similar in vitro anti-HIV activity to it (*31*, *32*).

Understanding why βFddA (**2**) and not αFddA (**1**) is effective against HIV represents a significant challenge since all structure−activity correlations with antiretroviral nucleosides are complicated by the complexity of the anabolic process of nucleoside activation. This process involves three or more sequential enzymatic steps that convert each nucleoside to its 5′-triphosphate, plus the final interaction of the 5′-triphosphate with the target enzyme, reverse transcriptase (RT) (*33*). We propose that it is only after discerning the conformational preferences exhibited by each nucleoside (or its intermediate nucleotide) at every intermediate stage, plus in the final step with RT, that one can explain the activity differences of these two diastereoisomers.

Recent studies by Meier et al. showed that for the anti-HIV inactive compound αFddA (**1**), circumvention of the activation step(s) with a prodrug of αFddAMP regained anti-HIV activity (*9*). This outcome was probably the result of the prodrug overcoming the rapid deamination of αFddA by adenosine deaminase (ADA) (vide infra) and/or its ineffective activation to αFddAMP. On the basis of NMR studies performed in our laboratory, we have demonstrated that αFddA (**1**) in solution prefers the north ($P = -0.2°$) conformation rather than the south conformation by an overwhelming ratio of 99:1 (Figure 2) (*13*). On the other hand, βFddA (**2**) prefers the antipodal south ($P = 132.7°$) conformation by 81% (Figure 2) (*13*). βFddA shows distinctly higher affinity than ddA for direct phosphorylation by deoxycytidine kinase (dCK) (*34*), and significant levels of the active βFddATP metabolite are eventually formed directly by this mechanism or indirectly by a 5′-nucleotidase-catalyzed phosphorylation step acting on the deaminated product (βFddI) (*35*−*38*). More importantly, greater intracellular concentrations of βFddATP are achieved relative to those of ddATP derived from the activation of ddA (*36*−*38*). We have also demonstrated that the catabolic enzyme ADA has the opposite diastereoisomeric preference (*13*). ADA significantly prefers to deaminate north-biased αFddA ($k_{cat}/K_m = 5.2\ \mu M^{-1}\ s^1$) over the epimeric south-biased βFddA ($k_{cat}/K_m = 0.08\ \mu M^{-1}\ s^1$) with a 65-fold greater catalytic efficiency (*13*). These combined observations suggest that while ADA prefers to bind to north αFddA (*13*), dCK binds effectively to the antipodal south conformation presented by βFddA (*34*).

Relative to the final sugar-related step—the conformational preference of RT—results from the AZT series utilizing conformationally rigid AZT-5′-triphosphate (AZTTP) analogues demonstrated a clear preference by RT for the north conformer of AZTTP (*3*, *4*). A similar preference for north AZTTP was recently confirmed by NMR (*39*), and the recent X-ray structure of the ternary complex of RT, double-stranded DNA, and bound dTTP (*40*) shows the incoming dTTP as a north conformer. Therefore, among the ensemble of enzymes involved in the entire process, the first kinases and RT appear to have opposite conformational preferences. Since βFddA (**2**) and αFddA (**1**) are conformationally biased to opposite ends of the pseudorotational cycle, and they represent good examples of compounds effectively discriminated by ADA (*13*) and possibly by dCK (*34*), we decided to determine whether the RT conformational preferences were also distinct for the two fluoronucleotides. This was particularly important in view of the aforementioned activity of the otherwise inactive αFddA diastereoisomer that was recovered by the prodrug approach (*9*).

On the basis of RT's preference to bind the north conformer of AZTTP (*4*, *39*), we hypothesized that αFddATP, which was shown to exist as a north conformer, would be a more potent inhibitor of RT than its south counterpart, βFddATP. A close examination of the mechanism of RT and the results from the X-ray structure of the ternary complex (vide supra) provided additional incentives to pursue this investigation (*40*, *41*). RT is a virally encoded multifunctional, RNA- and DNA-dependent DNA polymerase that is responsible for copying the single-stranded viral RNA genome into double-stranded DNA (*42*). Unlike most cellular polymerases, RT incorporates nucleotide analogues lacking a 3′-OH into the growing DNA chain (*33*). Once incorporated, these nucleotides block further elongation of the primer causing inhibition of viral replication (*33*). This very simple mechanism, however, does not explain why only a specific group of nucleoside analogues are endowed with important anti-HIV activity, while other structurally related compounds appear totally inactive (vide supra). The recently solved X-ray structure of the ternary complex of HIV-1 RT showing the stalled enzyme as a complex with an incoming dTTP at the active site demonstrated that although the DNA appears to be predominantly in the B-form, the base pairs close to the polymerase active site have an A-like conformation with a widened minor groove (*40*). It is important that in B-DNA, the 2′-deoxysugars prefer a distinct south conformation, whereas in A-DNA the 2′-deoxysugars require puckering in the antipodal north conformation (*17*). Therefore, if preference for the north conformation of DNA at the polymerase site is also extended to the dNTP (or ddNTP) binding site, as inferred from our earlier studies with conformationally rigid AZT analogues (*4*), we would expect a priori that αFddATP will be a better inhibitor of RT than βFddATP. However, the results showed that although both 5′-triphosphates inhibited RT, the order of potency, relative to ddATP, was ddATP > βFddATP > αFddATP. Earlier studies have shown that βFddATP is approximately 10-fold less potent as an inhibitor of RT than is its parent compound ddATP (*36*), with the difference being template-dependent (*38*). This can be understood in terms of the overwhelming preference of βFddATP for a south conformation. For αFddATP, on the other hand, the result contradicts our hypothesis. This study demonstrates that while RT clearly shows a preference to bind a north dNTP (or ddNTP), the tight dNTP binding pocket restricts the binding of north αFddATP in a manner similar to the way the enzyme effectively excludes the binding of ribonucleoside 5′-triphosphates (*40*, *43*) through a repulsive interference between Tyr115 and the axial 2′-C−F bond. This fluorine atom occupies the same relative position as the 2′-OH in a ribonucleoside 5′-triphosphate.

The most flexible of all the inhibitors, ddATP, is clearly the most effective because it can adapt to the spatial constraints of the enzyme's active site by flipping to a north conformation with a small energy penalty. Next is the conformationally south-biased βFddATP, which albeit able to bind to RT without interference from Tyr115 has to pay a higher energy penalty than ddATP to be flipped to the north conformation at the active site. Finally, the north-biased αFddATP has difficulty staying in its preferred north conformation because of the serious steric hindrance by Tyr115 at the active site.

MATERIALS AND METHODS

Synthesis of αFddATP and βFddATP. Each starting nucleoside (0.015 g, 0.059 mmol) was dissolved in trimethyl phosphate (0.4 mL) and cooled to 0 °C under an atmosphere of argon. Phosphorus oxychloride (60 μL, 0.632 mmol) was added and the solution was stirred for 3 h at 0 °C. The reaction was removed from the ice bath and treated immediately with tri-*n*-butylamine (0.37 mL), tri-*n*-butylammonium pyrophosphate (1.0 g, 1.83 mmol) dissolved in dry diethylformamide (4 mL), and triethylammonium bicarbonate (TEAB, 1 M) buffer (7.5 mL, pH 8.5). The resulting mixture was stirred at ambient temperature for 1 h, concentrated to dryness, redissolved in water (50 mL) and reduced to dryness again under vacuum for 14 h. The residue was dissolved in TEAB (2 mL, 0.01 M) and applied to a chromatography column (Pharmacia DEAE Sephacel, 2 × 25 cm, TEAB 0.01 M buffer). Two linear gradients of TEAB (400 mL, 0.01 → 0.1 M) and (600 mL, 0.1 → 0.6 M) were used in succession to elute the product. Major peaks absorbing at 254 and 280 nm were monitored using a Pharmacia dual path UV monitor and collected. The identity of the triphosphates was confirmed by HPLC analysis performed as described below. The triphosphates were further purified by column chromatography (Analtech, bonded C-18, 35−75 μ, 1.75 × 10 cm, 0.01 M TEAB) and the product-containing fractions were lyophilized, dissolved in water, and eluted through a Dowex 50 X8-100 (Na^+) ion-exchange resin (50 mL) with water. The corresponding sodium salts were obtained as white solids after lyophilization (0.014−0.020 g, 41−48%). HPLC analysis was performed using a Whatman Partisil 10 SAX (4.6 × 250 mm) anion-exchange column with a Waters WISP model 712 autosampler, two model 510 HPLC pumps and a Waters model 440 absorbance detector (@ 254 nm) connected in series to a Waters model 994 photodiode array detector. The samples were eluted with a mobile phase initially of 0.01 M $(H_4N)H_2PO_4$, native pH, for 15 min followed by a 25-min linear gradient to 0.7 M $(H_4N)H_2PO_4$/10% MeOH (native pH) that was maintained for 5 min, finally returning to initial conditions in 6 min using a linear gradient. The column was allowed to equilibrate for 9 min prior to the next injection. Instrument control, data analysis, and storage were accomplished using a Waters Millennium V2.1 chromatography

software run on a NEC Image 466 PC. Under these conditions, the predominant αFddATP peak (area = 86.6%) eluted with a retention time of 37.2 min, while the predominant βFddATP peak (area = 90.7%) eluted with a retention time of 39.5 min. The amount of diphosphate in each compound (t_R = 27.8 and 29.9 min) was ca. 9.5 and 7.6%, respectively.

Each sample was weighed accurately and brought to a volume with water (HPLC-grade) to give a final concentration of 1.0 mg/mL. For HPLC analysis, samples (usually 100 μL) were injected neat on-column. For UV spectrometry, samples were diluted 1:10 in 0.1 M phosphate buffer, pH 7.0. Concentrations were determined by measuring the absorbance using a fixed wavelength at the UV maxima of ATP (λ_{max} = 259, ϵ = 14 488, pH = 7) (*44*). Assuming a molecular weight of 599.12 (tetrasodium salt monohydrate), the amount of contamination due to unlyophilized salts was less than 20 wt % in each sample.

NMR Pseudorotational Analysis. NMR spectra were obtained at 25−35 °C on a Bruker AMX500 operating at 500 MHz for ^{1}H with a triple resonance gradient probe (S/N on 1H ∼ 650:1). ^{19}F-decoupled spectra were acquired at 470.59 MHz with a dual selective 1H/19F probe. ^{31}P-decoupled spectra were acquired at 202 MHz with an inverse broadband probe. Samples were dissolved either in D_2O at native pH or in D_2O adjusted to pH 4.0−5.0 with DCl. Both ^{1}H-coupled and broadband decoupled ^{19}F spectra were obtained to compare with simulated multiplets. One-dimensional ^{1}H spectra used for coupling constant analysis were acquired with 64 K data points and zero-filled to 128 K with a sweep width of 5050 Hz and a relaxation delay of 2 s. Temperature control at 500 MHz was provided by a Eurotherm VT unit with fluctuations of no more than 0.1 K. Spectra were processed with resolution enhancement using Gaussian multiplication (lb = −1, gb = 0.1). For first-order resonances, coupling constants were read directly from the resolution-enhanced spectra, while more complex multiplets were analyzed by spectral simulation using gNMR (Cherwell Scientific, Oxford, Great Britain). Simulation of the eight spin systems was performed with the fluorine resonance set 100 ppm upfield of the nearest proton multiplet. Rotamer populations around the C4′−C5′ bond (angle γ) were calculated as described (*45*). The ring conformations were analyzed with the program PSEUROT (*46*) v.6.2 (DOS version, purchased from Professor Cornelis Altona, University of Leiden, Leiden, The Netherlands) running on a Pentium II 333 MHz personal computer. The standard values supplied with version 6.2 for substituent electronegativities were used in the iterations (1.37 for fluorine). The calculations were performed essentially as described previously (*13*). The quality of the data was measured by the rms deviation of the calculated and experimental coupling constants. The rms deviation for the 5′-monophosphates was excellent (less than 0.4 Hz) indicating the parametrization of the program is well-suited to the input data. The 5′-triphosphates gave poorer rms deviations, and only αFddATP had a deviation slighlty above 0.4 Hz.

Inhibition of HIV-1$_{LAI}$ Reverse Transcriptase. Concentrations of αFddATP and βFddATP that reduce enzyme activity by 50% (IC_{50}) in the reverse transcriptase inhibition assay were determined using a previously published method (*47*, *48*) with some modifications (Table 3). Briefly, the reaction mixture was prepared to contain 50 mM Tris-HCl (pH 8.3), 10 mM $MgCl_2$, 100 mM KCl, 20 mM EGTA, 0.01% Triton X-100, 2.5 μM [^{3}H]dTTP, 20 μM of each of the remaining dNTPs, 0.25 μM MS2/22A [a heteropolymeric template-primer consisting of phage MS2 genomic RNA (Boeringer Mannheim, Indianapolis, IN) and the synthetic oligonucleotide, 22A (5′-CGT TAG CCA CTC CGA AGT T-3′) as a primer], reverse transcriptase, and 10-fold serially diluted concentrations of test compounds. Reactions were initiated by raising the reaction temperature from 0 to 37 °C. The reaction mixtures were incubated for 30−60 min at 37 °C and terminated by the addition of 250 mL of 10% trichloroacetic acid as a washing medium. All the assays were performed in triplicate. The IC_{50} values shown in Table 3 were used to calculate geometric means (the antilog of the mean of the logarithm of the values) with ranges. The geometric means of IC_{50} values (and ranges) of αFddATP and βFddATP were 50.1 μM (22.4−112.2) and 12.0 μM (8.9−16.2), respectively.

Molecular Dynamics Simulations. The crystal structures of βFddA (*25*) and ddA (*49*, *50*) were obtained from appropriate references and the Cambridge Structural Database. The structure of αFddA was built using QUANTA 97 on a Silicon Graphics O2 workstation running the IRIX 6.3 operating system, utilizing the CHARMm25 (MSI, San Diego, CA) force field. The conformation of αFddA was selected from a previous conformational search using QUANTA implemented tools (*13*). A starting conformation of αFddA with a glycosyl bond χ = −123.9° (anti), a pseudorotational phase angle P = 19.5° (north), and a torsion angle γ = 54.5° (+*sc*) was selected. As in our previous study with adenosine deaminase (*13*), the selection of a specific starting conformation was found not affect the final results. The ternary crystal structure of the RT-DNA-dTTP complex (PDB code 1RTD) was downloaded from the PDB databank. The protein was trimmed of all residues farther away than 10 Å from the active site. An 8-Å shell of water was added to the trimmed complex to prevent the majority of the DNA being exposed to vacuum. Atom constraints were added to atoms 4.0 Å away from the 5′-triphosphate (ddNTP) to prevent the added water from penetrating into the active site. The stability of the truncated RT−DNA−dTTP complex was confirmed by performing molecular mechanics energy minimization and molecular dynamics simulation. Complexes were minimized for 3000 steps using CHARMm 25 with version 2.2 of the force field parameters before performing molecular dynamics simulations. An adopted Newton−Raphson algorithm was used for energy minimization. The nonbonded interactions cutoff was set to 14.0 Å, a shift function was used to smooth the transition for the van der Waals interactions, and a force switch function was used for the electrostatic interactions. The cutoff distance parameters used in the smoothing functions are CTOFNB = 12.0 and CTONNB = 8.0 (*51*). All inhibitors were docked into RT using QUANTA. Molecular dynamics simulations on RT−DNA−ddNTP (ddNTP = ddATP, αFddATP and βFddATP) were performed with CHARMm25 on several Alpha CPU-based Linux systems by heating from 0 to 300 K over 5 ps and equilibrating at 300 K for an additional 10 ps. Production dynamics simulations were carried out for 500 ps with a step size of 0.001 ps at 300 K. Trajectories were recorded every 0.1 ps during the simulations. A shake

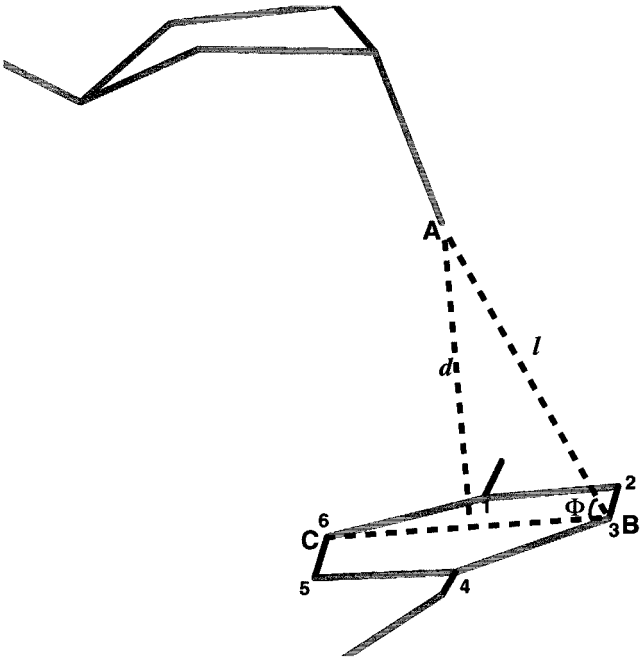

FIGURE 3: Diagram illustrating the method of triangulation to calculate the distance between H2″ and C2′−F to the center of the aromatic ring of Tyr115.

algorithm was used to constrain covalent bonds to hydrogen to 1×10^{-8} Å. Distances between atoms were taken as measured with QUANTA tools. Distances between hydrogen (H2″) or fluorine to Tyr115 were approximated using eqs 1 and 2 as depicted in Figure 3. In eq 1, d_i is the distance between hydrogen or fluorine and Tyr115 of the *i*th conformation; l_i is the distance between H″ (or the α-F in αFddATP) and a carbon selected on the tyrosine ring that is closest to them. *A* is the H″ hydrogen (or α-F), *B* is the selected carbon on Tyr115 that is closest to *A*, and *C* is the carbon diagonally opposite to atom *B*.

$$d_i = l_i \sin \phi_i \quad (1)$$

$$\phi_i = <ABC \quad (2)$$

RESULTS AND DISCUSSION

Pseudorotational Analysis of αFddA and βFddA 5′-Phosphate Esters. We have already reported the results of an NMR conformational analysis for *β*FddA and αFddA (*13*). For the present structure−activity analysis with RT, we confirmed that the preferred conformation of each nucleoside was faithfully maintained as their 5′-phosphate esters. This was verified by PSEUROT (*46*) analysis of the ^{1}H NMR spectra of *β*FddAMP, αFddAMP, and the corresponding 5′-triphosphates (Table 1). The spectral differences between *β*FddA and both *β*FddAMP and *β*FddATP are minimal and relate mostly to changes in chemical shift and minor changes in the fraction populated by the torsion angle *γ* (+*sc*, *ap*, −*sc*, Table 1). In the case of αFddAMP and αFddATP, extraction of accurate coupling constants was hampered by the complexity and degeneracy of the H3′, H″ region of the spectrum. This was partially resolved by spectral simulation and decoupling experiments. A fit of the data revealed a similar trend as was shown for the nucleosides (*13*): at, or near room temperature, the north conformation (%N, Table 1) seems to be overwhelmingly preferred for the αFddA nucleotides, whereas the *β*FddA nucleotides are biased toward the south conformation. On the basis of these data, we conclude that phosphorylation of *β*- and αFddA has little if any effect on furanose ring pucker and that the pseudorotational parameters are still dictated largely by the electronic character of the fluorine atom in these analogues.

Table 1: Conformational Data for αFddA and *β*FddA 5′-Mono- and 5′-Triphosphates[a]

compound	P_N	ν_N	P_S	ν_S	%N	rms[b]	γ^+	γ^t	γ^-
*β*FddAMP	−17.1	38.0[c]	133.4	38.0[c]	23	0.344	0.320	0.472	0.208
αFddAMP[d]	−9.6	35.0	180.0[c]	38.0[c]	100	0.238	0.680	0.293	0.027
*β*FddATP	−16.5	38.0[c]	133.6	38.0[c]	20	0.382	0.416	0.484	0.100
αFddATP[d]	−6.0	35.7	180.0[b]	36.0[c]	98	0.425	0.700	0.269	0.031

[a] *P* and *υ* values calculated with the program PSEUROT 6.2 (ref *46*). [b] Root-mean-square deviation between calculated and experimental coupling constants (Hz). [c] This parameter was fixed during the calculations. [d] Data obtained at 35 °C to resolve spectral overlap observed at 25 °C.

Molecular Docking of αFddATP and βFddATP at the Active Site of HIV-1 RT. The general shape of the polymerase domain of HIV-1 RT and other polymerases can be likened to a right-hand with subdomains referred to as fingers, palm, and thumb (*40*, *41*). A comparison between the structure of the ternary (RT−DNA−dNTP) and the binary (RT−DNA) complex revealed that the binding of a dNTP (or ddNTP) induces a substantial conformational change in HIV-1 RT where part of the fingers subdomain rotate inwardly toward the palm subdomain and the polymerase active site (*40*, *41*). As a result of this movement, two conserved amino acids (Lys65 and Arg72) form salt bridges with the *γ*- and α-phosphates, respectively, of the incoming dNTP (or ddNTP). This rearrangement that takes place upon dNTP or (ddNTP) binding to HIV-1 RT creates the so-called "3′ pocket" where the 3′-OH of the incoming dNTP is aligned with the side chains of conserved residues such as Ala114, Tyr115, and Gln151. Since ddNTP inhibitors of RT lack a 3′-OH group, the 3′ pocket plays an important role in accommodating either bulkier molecules such as AZTTP, with a large azido group, or the smaller and more flexible ddNTPs that have no substituent at the 3′-position (*40*). The structure of the complex also shows that the dNTP (or ddNTP) binding site is tight and thus capable of discriminating changes in size and shape, as well as preferences for a specific form of sugar pucker (vide infra).

To study the fit of ddATP, αFddATP, and *β*FddATP into the dNTP-binding site, the ternary complex of RT−DNA−ddATP was first modeled with ddATP as a prototype. As shown in Figure 4, this complex showed similar binding characteristics as seen in the X-ray structure of the RT−DNA−dTTP (shown in light yellow) (*40*), except for the reversal of the A−T base pair. The two hydrogen bonds between A and T are shown to have the ideal distances and angles to form a strong Watson−Crick base pair, and the ribose ring maintains a similar position relative to Arg72, Gln151, and Lys65. Interestingly, while the south X-ray structure of ddA (*49*, *50*) was initially used for docking ddATP at the RT site, the conformation switched to north after energy minimization. Furthermore, the dideoxyribose ring remained in a north conformation during 500 ps of

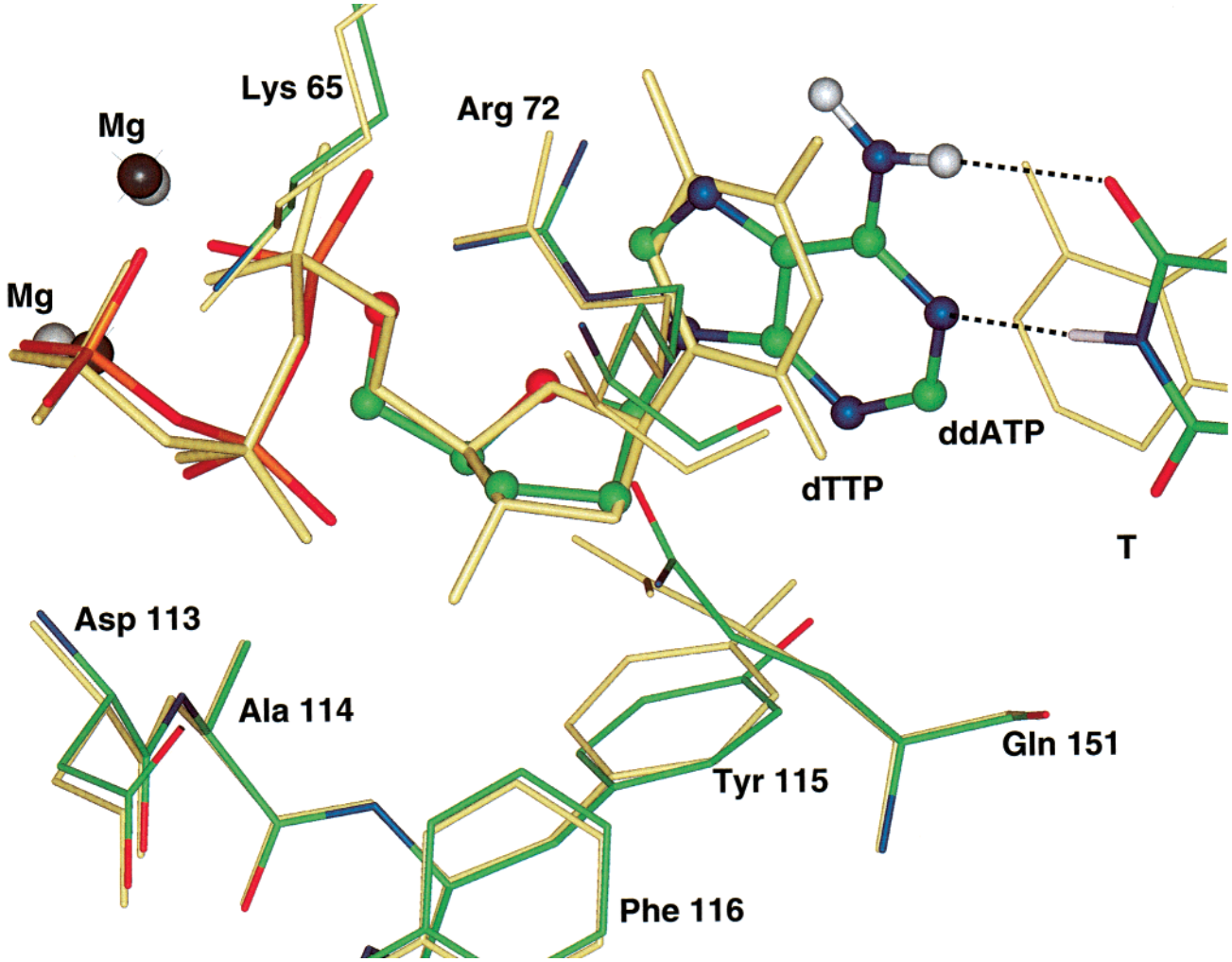

FIGURE 4: Static view of the dNTP binding site of our model of RT in complex with ddATP, superposed on the crystal structure of RT−DNA−dTTP.

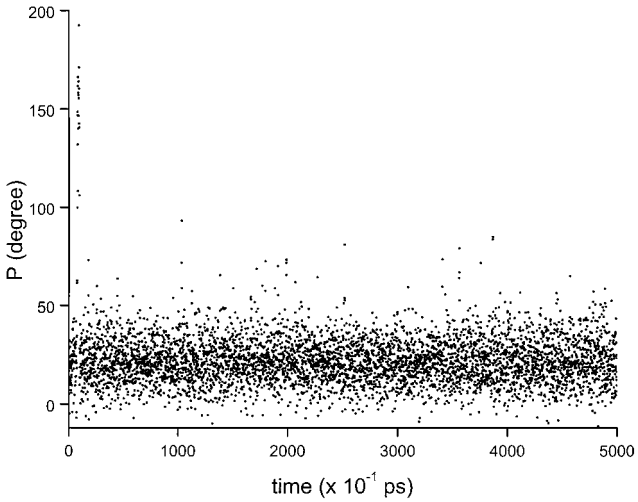

FIGURE 5: Molecular dynamics simulation showing the conformational change (*P*) of the dideoxyribose ring of ddATP in a ternary complex with RT.

dynamic simulation, except for a brief 1 ps (8th picosecond) where it flipped to a south conformation (Figure 5). About 94% of the trajectories recorded from the dynamics simulation show the dideoxyribose ring with *P* values ranging from 320 to 40°. Within that cluster, nearly half of the population shows a pure form of north pucker with $P = 0-20°$ (Table 2, Figure 5). During the same dynamics simulation the distance between the 2″-H and Tyr115 (see experimental) fluctuates almost symmetrically from a mean value of 2.4 Å revealing no particular steric stress (Figure 6). Therefore, in the north conformation the dideoxyribose appears to fit tightly into the active site with the 2″-H close to, but not colliding, with Tyr115.

Table 2: Dideoxyribose Ring Conformation Distribution of ddATP, αFddATP, and βFddATP Complexed with RT during 500 ps of Dynamics Simulation

	no. of frames		
P range (°)	ddA	αFddA	βFddA
0−20	2179	30	3111
20−40	2431	396	724
40−60	262	1211	548
60−80	21	1420	196
80−120	7	1345	22
120−160	10	516	0
160−200	6	77	0
200−240	1	0	0
240−280	0	0	0
280−320	0	0	0
320−340	83	2	399

The binding of αFddATP to RT presents an interesting dilemma for RT since the preference for a north conformation causes a steric clash between the aromatic ring of Tyr115

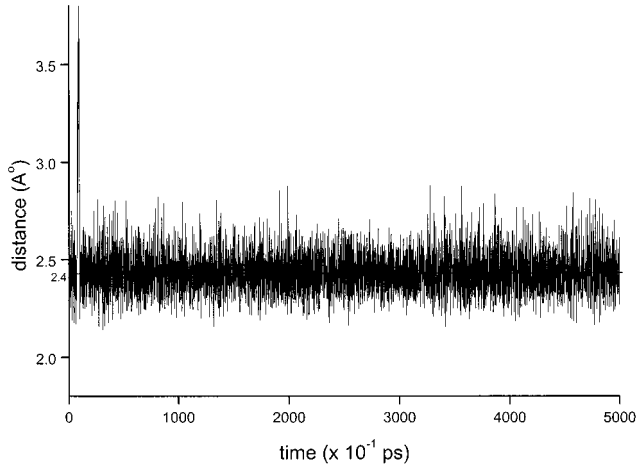

FIGURE 6: Fluctuating distances between the H2″ of ddATP and Tyr115 in the ternary complex during the entire simulation.

and the axially disposed α-fluorine 2.4 Å away (Figure 7). To avoid such a clash, the enzyme has to squeeze the dideoxyribose ring toward an east ($P = 90°$) or even to a south conformation (Figure 7). As shown in Table 2 and Figure 8, 80% of the value of P during the 500 ps dynamics simulation appears distributed between 40−120°, with two-thirds of the values concentrated in the narrow 60−80° region. The evolution of P during the dynamics simulation clearly shows that αFddATP tries to adopt a north conformation, but it is rapidly forced to change to a south conformation when confronted with the high energy barrier of the complex represented by the proximity to Tyr115. A cursory visual inspection of Figure 8, as compared to the more steady tracing of ddATP in Figure 5, provides convincing evidence of the struggle that it represents for αFddATP to find an accommodating conformation at the active site. A trace of the distance between the fluorine atom in αFddATP and the center of the aromatic ring of Tyr115 (see experimental) indicates that the repulsive barrier appears at ca. 2.4 Å (Figure 9). When the dideoxyribose ring oscillates between north and south, the distance of the C2′−F and Tyr115 fluctuates asymmetrically between 2.4 and 3.9 Å as if the molecule were bouncing against a wall. Noticeably, there is little room for Tyr115 to dodge the collision by turning the aromatic ring off its original plane (Figure 7). Also observed in Figure 7 is that the surrounding residues at the active site respond very little to the north−south changes of the dideoxyribose ring. However, the displacement of the adenine base from a pseudoaxial (north) to a pseudoequatorial (south) position shows a visible translation that might slightly alter base pair interactions (Figure 7, dotted lines).

When the C2′-fluorine is switched to a position above the plane of the dideoxyribose ring, as in βFddATP, again we have opposing forces at work. Clearly, the previously discussed steric clash between fluorine and Tyr115 is no

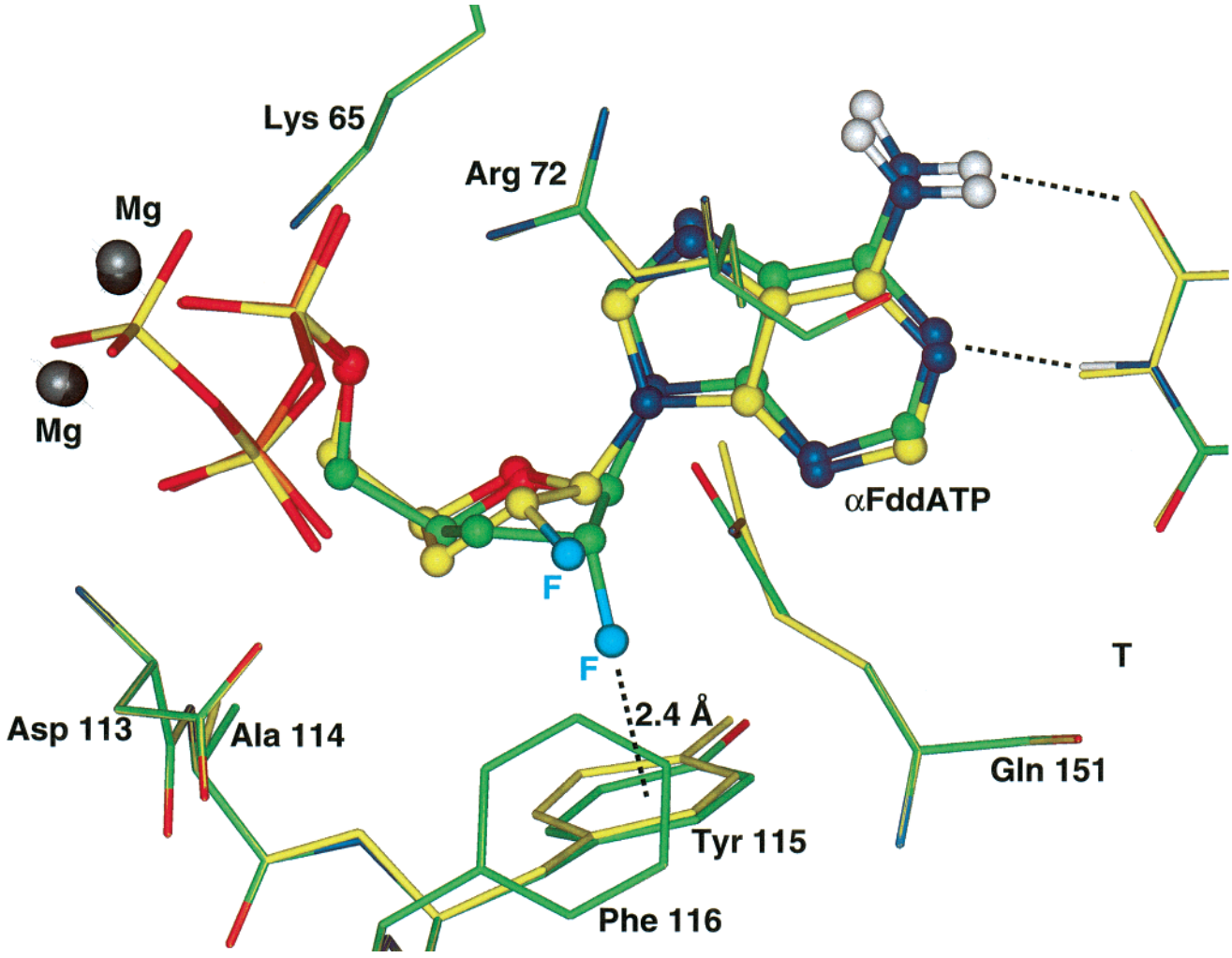

FIGURE 7: Static view of the dNTP binding site of RT in complex with north and south αFddATP.

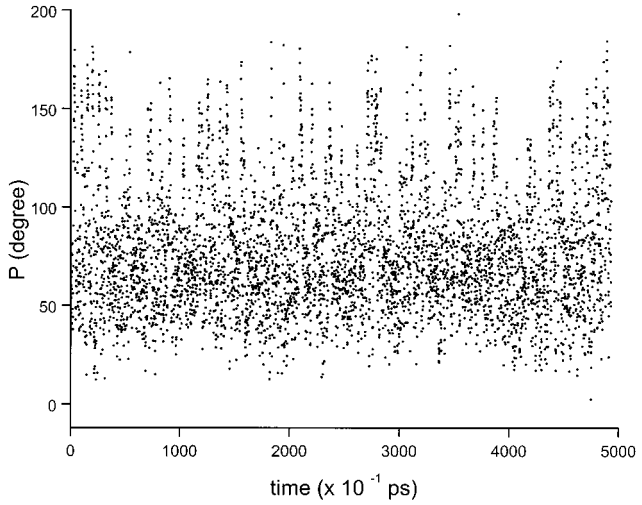

FIGURE 8: Molecular dynamics simulation showing the conformational change (*P*) of the dideoxyribose ring of αFddATP in a ternary complex with RT.

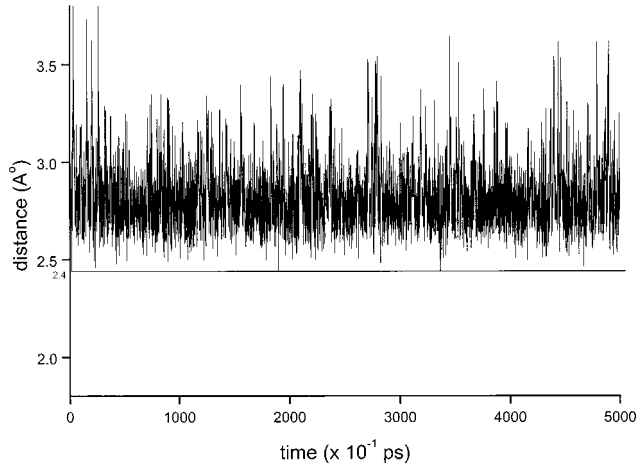

FIGURE 9: Fluctuating distances between the 2′-F of αFddATP and Tyr115 in the ternary complex during the entire simulation.

longer an issue (Figure 10). Moreover, when RT forces βFddATP to adopt a north conformation—against its natural tendency—an electrostatic attraction between the positive Arg72 and the polarized C−F bond might further stabilize the ligand in the north conformation. In general, βFddATP behaves similarly to ddATP, except that the energy price for flipping into the north conformation is higher due to the strong opposition of the fluorine in βFddATP that favors a stable south conformation as a result of the gauche effect (*18*). This is probably reflected in the fact that it took longer for βFddATP to reach a stable north conformation during the dynamics simulation. In contrast, finding a comfortable north conformation for ddATP was almost instantaneous (Figure 5), while for βFddATP, the dideoxyribose ring flipped to stable north conformation in the complex only after about 100 ps of adjusting *P* and γ (Figure 11, γ not shown). For βFddATP, about 85% of the *P* values ranged from 40−320°, while more than 72% of the population concentrated around a pure north ($P = 0-20°$ region, Table 2, Figure 11). For the 15% of *P* values ranging from 40−80°, 80% were recorded from the first 100 ps simulation (Figure 11). Importantly, throughout the 500 ps dynamics simulation of βFddATP, the fluorine did not bump into any residue, and the H-2″ hydrogen did not collide with Tyr115. However, when comparing the trace of the fluctuating distances between both H-2″ hydrogens in ddATP and βFddATP to Tyr115, βFddATP appears to fit less comfortably into the site (compare Figures 6 and 12). As in the case of ddATP, the initially docked structure of βFddATP was based on the available south X-ray crystal structure of βFddA (*25*). Figure 10 compares two static complexes with βFddATP in the extreme north ($P = 0°$) conformation and in the extreme south ($P = 180°$) conformation with RT−DNA. As before, the amino acid residues appear to react only slightly to the changes in conformation while the adenine bases do not superimpose. Although the static complexes do not provide any insight in resolving which conformation of βFddATP is preferred, the molecular dynamics simulation for βFddATP reflects how the structure adjusted from the initial crystal structure in the South conformation (*25*) to an optimal, preferred north conformation at the active site demanded by RT.

Inhibition of HIV-1 Reverse Transcriptase by βFddATP and αFddATP. Reverse transcription represents an essential step for retroviral replication (*33*, *42*). In this critical step, substrate binding is ordered: nucleic acid template−primer binding is followed by the high affinity binding of the correct 2′-deoxynucleoside 5′-triphosphate complementary to the next position on the template (*41*). Incorporation of the new nucleotide unit into the nascent chain then occurs via S_N2 displacement of the pyrophosphate by the 3′-OH of the preceding nucleotide unit. Misincorporation of a modified nucleotide lacking the 3′-OH moiety, such as βFddATP or αFddATP, results in premature chain termination and inhibition of the polymerase function of RT. As mentioned before, near the polymerase active site the template resembles canonical A-form DNA, whereas the template−dimer resembles B-form DNA (*40*, *41*). It is therefore anticipated that the incoming 5′-triphosphates would preferentially bind with a north sugar conformation characteristic of A-form DNA. Inhibition of reverse transcriptase by βFddATP and αFddATP was measured by a previously published method with some minor modifications (see Materials and Methods). A heteropolymeric template−primer consisting of phage MS2 genomic RNA and a synthetic oligonucleotide primer was used in the presence of various concentrations of αFddATP and βFddATP. IC_{50} values from four different experiments are presented in Table 3. Geometric means for βFddATP and αFddATP were calculated to be 12.0 and 50.1 μM, respectively, and the plot correlating DPM of [^{3}H]TMP incorporated versus drug concentration is shown in Figure 13.

Despite the demonstrated preference of αFddATP for a north conformation, which is compatible with the conformational characteristics of the polymerase active site, the results show that αFddATP is the poorer inhibitor of the two. This can be satisfactorily explained by the steric clash revealed by molecular dynamic simulations showing the difficulty of fitting a north αFddATP into the active site (vide supra). To avoid such a clash, the molecule shifts to the less stable south conformation. As a result of this tension between two opposite driving forces, the binding of αFddATP is not very effective. On the other hand, despite having a preference for a south conformation, βFddATP is able to eventually change to a stable north conformation at the active site, albeit

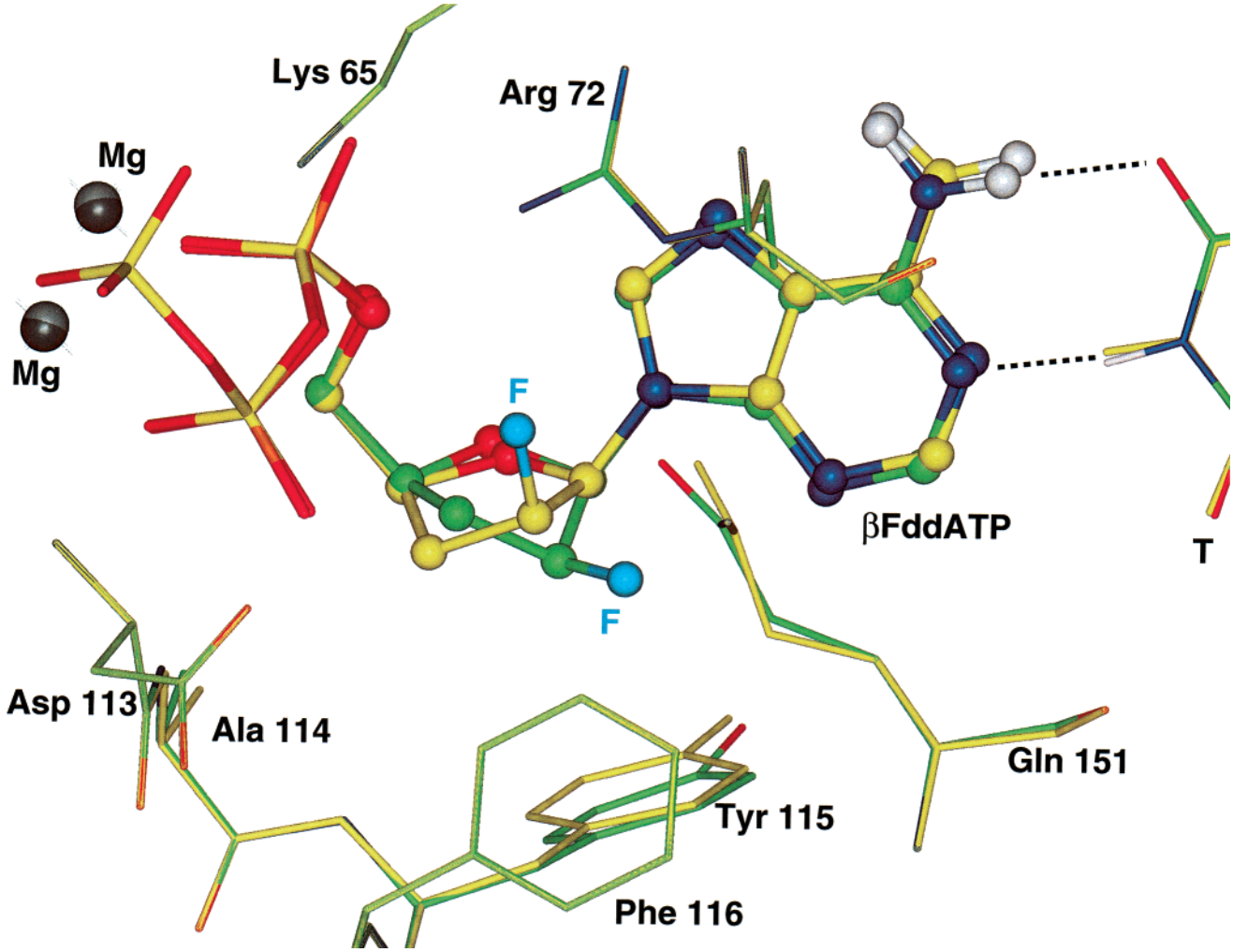

FIGURE 10: Static view of the dNTP binding site of RT in complex with north and south βFddATP.

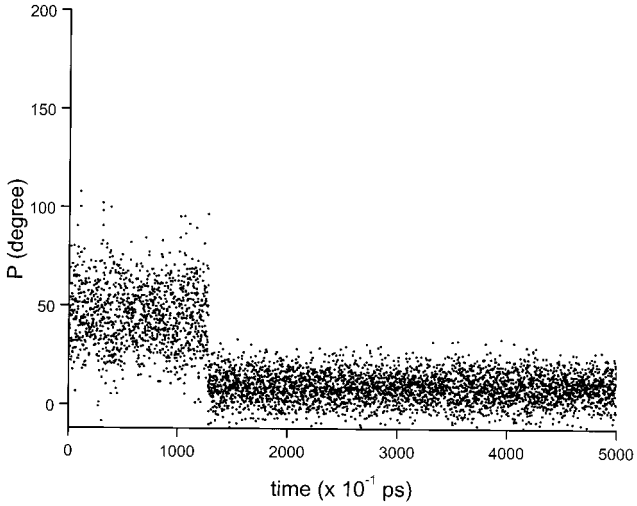

FIGURE 11: Molecular dynamics simulation showing the conformational change (*P*) of the dideoxyribose ring of βFddATP in a ternary complex with RT.

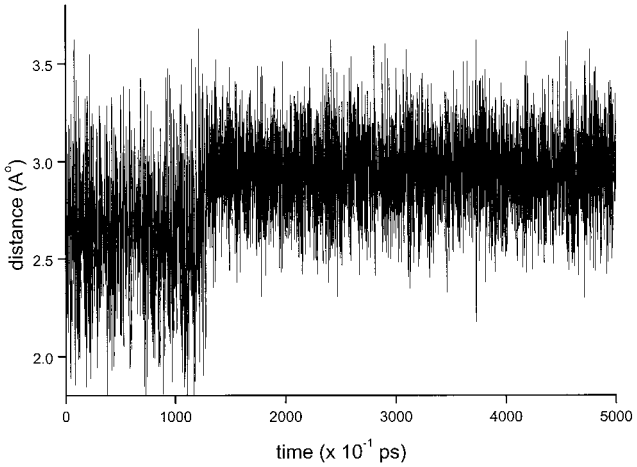

FIGURE 12: Fluctuating distances between the H2″ of βFddATP and Tyr115 in the ternary complex during the entire simulation.

with some penalty relative to an unencumbered dideoxynucleoside, such as ddATP. While not ideal, this situation is energetically more attainable and therefore compatible with the experimental data showing βFddATP being ca. 4 times more potent than αFddATP as inhibitor of RT. The same rationale explains why ddATP is the most potent inhibitor of the three. Because of the absence of fluorine, ddATP can switch to a north conformation with a smaller energy penalty than βFddATP. In practice, the potential therapeutic advantage of βFddA over ddA, in addition to its chemical and enzymatic stability (*30*, *31*, *34*, *36*−*38*), derives from the higher levels accrued of the critical metabolite, βFddATP, that results from the conformational preference of the kinases (e.g., dCK) for the south conformation of βFddA (*34*, *36*−*38*).

Table 3: Inhibition (IC_{50}) of HIV-1 RT by βFddATP and αFddATP

	IC_{50} (μM)			
compound	exp 1	exp 2	exp 3	exp 4
βFddATP	15.3	7.3	10.2	15.8
αFddATP	62.9	15.8	29.4	191.5

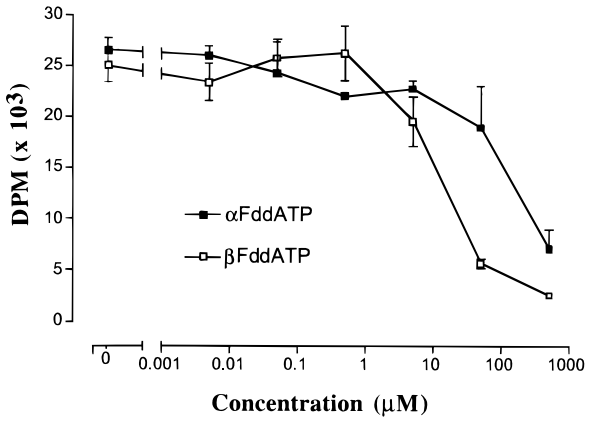

FIGURE 13: Inhibition of HIV RT by αFddATP and βFddATP. Results are expressed as DPM of [^{3}H]TMP incorporated.

CONCLUSION

Two important conclusions can be derived from this study: (i) the conformational preference for the incoming dNTP (or ddNTP) is to adopt a north conformation compatible with the A-like conformation of the DNA at the polymerase active site (this is strongly supported by the results of the dynamics simulation studies with bound ddATP); and (ii) the chemical nature and stereochemical orientation of the substituents on the dideoxysugar (i.e., fluorine), which influence the conformational preference of the sugar ring, play fundamental roles in controlling the final fit in terms of electronic and/or steric interactions with the surrounding amino acids at the active site. The results from molecular dynamics simulation with bound ddATP, βFddATP, and αFddATP explain the observed order of potency of the corresponding 5′-triphosphates as inhibitors of RT. The amino acid Tyr115, which appears to function as a steric gate to prevent the binding of riboside 5′-triphosphates in a tight environment (*43*), prevents the effective binding of αFddATP in the preferred north conformation. The north conformation, favored by RT and energetically preferred by αFddATP, is opposed by the strong repulsive clash between the fluorine and the aromatic ring of Tyr115. This phenomenon translates into a less-than-desirable fit and prevents αFddATP from having the best binding affinity for RT. The fact that RT can prevent the incorporation of riboside 5′-triphosphates while allowing αFddATP to bind reflects the differences in steric bulk between a C−F bond (1.379 Å) and the combined C−O and O−H bonds (C−O = 1.426 Å and O−H = 0.958 Å).

ACKNOWLEDGMENT

We thank Drs. John S. Driscoll and David G. Johns of this laboratory for critically reading the manuscript.

REFERENCES

1. Jeong, L. S., Marquez, V. E., Yuan, C.-S., and Borchardt, R. T. (1995) *Heterocycles 41*, 2651−2656.
2. Marquez, V. E., Siddiqui, M. A., Ezzitouni, A., Russ, P., Wang, J., Wagner, R. W., and Matteucci, M. (1996) *J. Med. Chem. 39*, 3739−3747.
3. Marquez, V. E., Ezzitouni, A., Russ, P., Siddiqui, M. A., Ford, H., Jr., Feldman, R. J., Mitsuya, H., George, C., and Barchi, J. J., Jr. (1998) *Nucleosides Nucleotides 17*, 1881−1884.
4. Marquez, V. E., Ezzitouni, A., Russ, P., Siddiqui, M. A., Ford, H., Jr., Feldman, R. J., Mitsuya, H., George, C., and Barchi, J. J., Jr. (1998) *J. Am. Chem. Soc. 120*, 2780−2789.
5. Jeong, L. S., Buenger, G., McCormack, J. J., Cooney, D. A., Hao, Z., and Marquez, V. E. (1998) *J. Med. Chem. 41*, 2572−2578.
6. Ikeda, H., Barchi, J. J., Jr., Wilk, A., Egli, M., and Marquez, V. E. (1998) *Nucleic Acids Symp. Ser. No. 39*, 57−58.
7. Ikeda, H., Fernandez, R., Wilk, A., Barchi, J. J., Jr., and Marquez, V. E. (1998) *Nucleic Acids Res. 26*, 2237−2244.
8. Berger, I., Tereshko, V., Ikeda, H., Marquez, V. E., and Egli, M. (1998) *Nucleic Acids Res. 26*, 2473−2480.
9. Meier, C., Knispel, T., Marquez, V. E., Siddiqui, M. A., De Clercq, E., and Balzarini, J. (1999) *J. Med. Chem. 42*, 1615−1624.
10. Marquez, V. E., Russ, P., Alonso, R., Siddiqui, M. A., Shin, K. J., George, C., Nicklaus, M., Dai, F., and Ford, H., Jr. (1999) *Nucleosides Nucleotides 18*, 521−530.
11. Marquez, V. E., Russ, P., Alonso, R., Siddiqui, M. A., Hernandez, S., George, C., Nicklaus, M. C., Dai, F., and Ford, H., Jr. (1999) *Helv. Chim. Acta 82*, 2119−2129.
12. Nandanan, E., Jang, S.-Y., Moro, S., Kim, H., Siddiqui, M. A., Russ, P., Marquez, V. E., Busson, R., Herdewjin, P., Harden, T. K., Boyer, J. L., and Jacobson, K. A. (2000) *J. Med. Chem. 43*, 829−842.
13. Ford, H., Jr., Dai, F., Mu, L., Siddiqui, M. A., Nicklaus, M. C., Anderson, L., Marquez, V. E., and Barchi, J. J., Jr. (2000) *Biochemistry 39*, 2581−2592.
14. Jacobson, K. A., Ji, X., Li, A., Melman, N., Siddiqui, M. A., Shin, K. J., Marquez, V. E., and Ravi, R. G. (2000) *J. Med. Chem. 43*, 2196−2203.
15. Prota, A., Vogt, J., Perozzo, R., Pilger, B., Wurth, C., Marquez, V. E., Russ, P., Schultz, G. E., Folkers, G., and Scapozza, L. *Biochemistry* (2000) *39*, 9597−9603.
16. Altona, C., and Sundaranlingam, M. (1972) *J. Am. Chem. Soc. 94*, 8205.
17. For a comprehensive review of these concepts see Saenger, W. (1984) *Principles of Nucleic Acid Structure*, Springer-Verlag, New York.
18. For a comprehensive review of these concepts see Thibaudeau, C., and Chattopahyaya, J. (1999) *Stereoelectronic Effects in Nucleosides and Nucleotides and their Structural Implications*, Uppsala University Press, Uppsala Sweden.
19. For a comprehensive review of these concepts see Marquez, V. E., Lim, B. B., Barchi, J. J., Jr., and Nicklaus, M. C. (1993) Conformational studies and anti-HIV activity of mono- and difluorodideoxy nucleosides. In *Nucleosides and Nucleotides as Antitumor and Antiviral Agents* (Chu, C. K., and Baker, D. C., Eds.) pp 265−284, Plenum Press, New York.
20. Camerman, N., Mastropaolo, D., and Camerman, A. (1990) *Proc. Natl. Acad. Sci. U.S.A. 87*, 3543−3537.
21. Everaert, D. H., Peeters, O. M., Blaton, N. M., and De Ranter, C. J. (1990) *Acta Crystallogr. C46*, 1730−1732.
22. Van Roey, P., and Schinazi, R. F. (1990) *Antiviral Chem. Chemother. 1*, 93−98.
23. Van Aerschot, A. A., Everaert, D. H., Peeters, O. M., Blaton, N. M, De Ranter, C. J., and Herdewjin, P. (1990) *Nucleosides Nucleotides 9*, 547−557.
24. Hayakawa, H., Takai, F., Tanaka, H., Miyasaka, T., and Yamaguchi, K. (1990) *Chem. Pharm. Bull. 38*, 1136−1139.
25. Liaw, Y.-C., Gao, Y.-G., Marquez, V. E., and Wang, A. H.-J. (1992) *Nucleic Acids Res. 20*, 459−465.
26. Cody, V., and Kalman, T. T. (1992) *Nucleosides Nucleotides 11*, 731−738.
27. Shutalev, A. D., Mikerin, I. E., Arshava, B. M., Nikitenko, A. A., Raifeld, Y. E., Vid, G. Y., Lee, V. J., Gurskaya, G. V.,

Viktorova, L. S., Jasko, M. V., Semizarov, D. G., and Zavodnik, V. E. (1994) *Bioorg. Med. Chem. Lett. 4*, 761−768.
28. Barchi, J. J., Jr., Jeong, L. S., Siddiqui, M. A., and Marquez, V. E. (1997) *J. Biochem. Biophys. Methods 34*, 11−29.
29. Thibaudeau, C., Plavec, J., and Chattopadhyaya, J. (1998) *J. Org. Chem. 63*, 4967−4984.
30. Marquez, V. E., Tseng, C. K.-H., Kelley, J. A., Mitsuya, H., Broder, S., Roth, and Driscoll, J. S. (1987) *Biochem. Pharmacol. 36*, 2719−2722.
31. Marquez, V. E., Tseng, C. K.-H., Mitsuya, H., Aoki, S., Kelley, J. A., Ford, H., Jr., Roth, J. S., Broder, S., Johns, D. G., and Driscoll, J. S. (1990) *J. Med. Chem. 33*, 978−985.
32. Herdewijn, P., Pauwels, R., Baba, M., Balzarini, J., and De Clercq, E. (1987) *J. Med. Chem. 30*, 2131−2137.
33. For a comprehensive review of these concepts see Mitsuya, H. (1997) *Anti-HIV Nucleosides. Past, Present and Future*, Chapman & Hall, New York.
34. Eriksson, S., Kierdaszuk, B., Munch-Petersen, B., Öberg, B., and Johansson, N. G. (1991) *Biochem. Biophys. Res. Commun. 176*, 586−592.
35. Johnson, M. A., and Fridland, A. (1989) *Mol. Pharmacol. 36*, 291−295.
36. Masood, R., Ahluwalia, G. S., Cooney, D. A., Fridland, A., Marquez, V. E., Driscoll, J. S., Hao, Z., Mitsuya, H., Perno, C. F., Broder, S., and Johns, D. G. (1990) *Mol. Pharmacol. 37*, 590−596.
37. Fridland, A., Johnson, M. A., Cooney, D. A., Ahluwalia, G., Marquez, V. E., Driscoll, J. S., and Johns, D. G. (1990) *Ann. N. Y. Acad. Sci. 616*, 205−216.
38. Hitchcock, M. J. M., Woods, K., De Boeck, H., and Ho, H.-T. (1990) *Antiviral Chem. Chemother. 1*, 319−327.
39. Painter, G. R., Andrews, C. W., and Furman, P. A. (2000) *Nucleosides Nucleotides 19*, 13−29.
40. Huang, H., Chopra, R., Verdine, G. L., and Harrison, S. C. (1998) *Science 282*, 1669−1675.
41. Sarafianos, S. G., Das, K., Ding, J., Boyer, P. L., Hughes, S. H., and Arnold, E. (1999) *Chem. Biol. 6*, R137−R146.
42. Luciw, P. (1996) Human immunodeficiency viruses and their replication, in *Fundamental Virology* (Fields, B. N, Knipe, D. M., and Howley, P. M., Eds.) pp 845−916, Lippincont-Raven, New York.
43. Boyer, P. L., Sarafianos, S. G., Arnold, E., and Hughes, S. H. (2000) *Proc. Natl. Acad. Sci. U.S.A. 97*, 3056−3061.
44. Albert, A. (1973) The ultraviolet spectra of pyrimidines and purines in *Synthetic Procedures in Nucleic Acid Chemistry Vol. 2: Physical and Physicochemical Aids in Characterization and in Determninations of Structure* (Zorbach, W. W., and Tipson, R. S., Eds.) pp 47−123, Wiley-Interscience, New York.
45. Wu, G. D., Serianni, A. S., and Barker, R. (1983) *J. Org. Chem. 48*, 1750−1757.
46. Van Wijk, J., Huckriede, B. D., Ippel, J. H., and Altona, C. (1992) *Methods Enzymol. 211*, 286−306, and references therein.
47. Ueno, T., Shirakasa, T., and Mitsuya, H. (1995) *J. Biol. Chem. 270*, 23605−23611.
48. Tanaka, M., Srinivas, R. V., Ueno, T., Kavlick, M. F., Hui, F. K., Fridland, A., Driscoll, J. S., and Mitsuya, H. (1997) *Antimicrob. Agents Chemother. 41*, 1313−1318.
49. Chu, C. K., Bhadti, V. S., Doboszewski, B., Gu, Z. P., Kosugi, Y., Pullaiah, K. C., and Van Roey, P. (1989) *J. Org. Chem. 54*, 2217−2225.
50. Silverton, J. V., Quinn, F. R., Haugwitz, R. D., and Todaro, L. J. (1988) *Acta Crystallogr. C44*, 321−324.
51. CTOFNB, distance cutoff at which the switching function eliminates all contributions from a pair in calculating energies; CTONNB, distance cutoff at which the smoothing function begins to reduce a pair's contribution.

BI001090N